ELSEVIER

Journal of Nuclear Materials 299 (2001) 235–241

journal of nuclear materials

www.elsevier.com/locate/jnucmat

A working hypothesis on oxidation kinetics of Zircaloy

H.-I. Yoo [a,*], B.-J. Koo [a], J.-O. Hong [a], I.-S. Hwang [b], Y.-H. Jeong [c]

[a] *School of Materials Science and Engineering, College of Engineering, Seoul National University, Seoul 151-742, South Korea*
[b] *Department of Nuclear Engineering, Seoul National University, Seoul 151-742, South Korea*
[c] *Korea Atomic Energy Research Institute, Daejeon, South Korea*

Received 3 April 2001; accepted 28 August 2001

Abstract

A kinetic hypothesis of zirconium oxidation has been developed in a closed form by assuming a constant strain-energy gradient as a diffusional driving force in addition to an oxygen chemical potential gradient, and verified quantitatively via thermogravimetry in the air atmosphere over a temperature range of 400–800 °C. The hypothesis explains quite precisely the crossover of kinetics from parabolic to cubic before the breakaway of ZrO_2-scale, yielding an intrinsic diffusion coefficient of component oxygen as $D_O/m^2\ s^{-1} = 6.3 \times 10^{-9} \exp(-1.59\ eV\ kT^{-1})$. The open-circuit potential measurement across the protective scale indicates that the scale is a mixed ionic electronic conductor with an ionic transference number of $t_{ion} \approx 0.5$. The intrinsic diffusivity is thus interpreted as being a Nernst-type combination of the partial conductivities of oxide ions and electrons. The hypothesis also yields a strain-energy gradient across the protective layer of 10^{11} to 10^{10} J $m^{-1}(mol\text{-}O)^{-1}$ as temperature increases from 400 to 800 °C. The strain-energy gradient allows one to evaluate the characteristic thickness where the oxide breaks away, and the strain energy right at the ZrO_2/Zr interface to be very reasonably on the order of 10^{10} J m^{-3} that is insensitive to temperature. Possible origins of the stress are discussed.

PACS: 81.65.Mq

1. Introduction

Oxidation kinetics of Zircaloy have been a subject of extensive studies for the past 50 years, but the quantitative understanding of it is still at large. Nevertheless, it seems to be phenomenologically agreed upon [1,2] that the oxidation kinetics are very initially linear ($\Delta m \propto t$), followed often by a parabolic kinetics ($\Delta m \propto t^{1/2}$), but eventually by a cubic kinetics ($\Delta m \propto t^{1/3}$) until a final transition to a linear kinetics or breakaway. Microscopically, the oxide layer grown up to the transition or breakaway point (so-called pre-transition period) is dense and protective, but the layer after the transition (post-transition period) is non-protective bearing cracks and/or pores [3,4]. The protective layer normally extends over a limited thickness (of 2–3 μm or so) at temperatures of practical interest (~600 K) [2,3]. Crystallographically, the protective layer contains appreciable amount of tetragonal zirconia (t-ZrO_2) [3–6] at the temperatures where monoclinic zirconia (m-ZrO_2) should otherwise be stable thermodynamically. The non-protective porous layer, on the other hand, is always monoclinic [5,6].

It is well known that t-ZrO_2 can be stabilized over m-ZrO_2 even at room temperature by the effects of surface tension, hydrostatic pressure or compressive stress [7]. The presence of t-ZrO_2 in the protective layer is thus generally attributed to a compressive stress [5], but its origin has not yet been clearly understood [8]. Nevertheless, it can be envisaged that this compressive stress may play a role in oxidation kinetics. A few attempts have thus far been made to explain the kinetics by taking into account the stress gradient in addition to the oxygen concentration gradient as diffusional driving forces [9,10]; however the quantitative rationalization of the overall kinetics of Zircaloy oxidation is still rudimentary.

* Corresponding author. Tel.: +82-2 880 7163; fax: +82-2 884 1413.
E-mail address: hiyoo@plaza.snu.ac.kr (H.-I. Yoo).

0022-3115/01/$ - see front matter
PII: S0022-3115(01)00695-X

In this paper, we will propose a working hypothesis which can explain quantitatively the crossover of kinetics from parabolic to cubic, and provide the experimental evidence supporting the hypothesis. On the basis of this hypothesis, we will then discuss the nature of rate-determining diffusion through the reaction product, the characteristic features of the protective layer and the origin of the compressive stress.

2. Working hypothesis

Let us consider an infinite slab of Zr–metal (or Zircaloy) exposed to an ambient oxygen potential μ''_{O_2}, which is greater than the oxygen potential, μ'_{O_2} in equilibrium with Zr–metal and ZrO_2 at a given temperature. In addition, we conjecture that the oxide is somehow subjected to a compressive stress gradient starting from the Zr/ZrO_2 interface. The thermodynamic situation is as illustrated in Fig. 1.

It is well known [11] that oxidation of Zr proceeds via chemical diffusion of component oxygen from the free surface to the Zr/ZrO_2 interface. A flux of mobile component oxygen, J_O may be induced not only by the gradient of the chemical potential of component oxygen, $\nabla\mu_O$, but also by the gradient of (compressive) strain energy, ∇u [12] or

$$J_O = -L(\nabla\mu_O + \nabla u), \tag{1}$$

where the transport coefficient L is a measure of the intrinsic diffusion coefficient of component oxygen, D_O or

$$L = \frac{D_O C_O}{RT}. \tag{2}$$

Here, C_O is the (molar) concentration of oxygen in ZrO_2, and the other symbols have their usual significance.

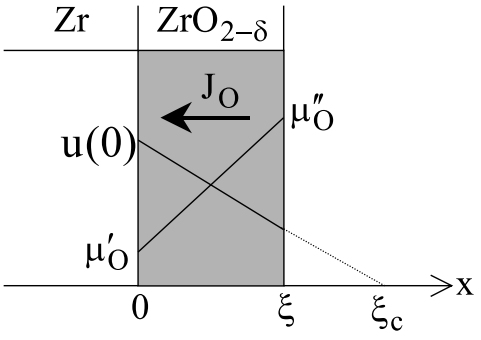

Fig. 1. Thermodynamic situation of Zr-oxidation. Note that the diffusion flux of component oxygen, J_O is driven by the chemical potential gradient of oxygen, $\nabla\mu_O$ and the (compressive) strain-energy gradient, ∇u which are acting in opposite directions. ξ, thickness of the reaction product; ξ_C, the characteristic thickness where $u = 0$.

If the (in-plane) compressive stress originates from the lattice or interfacial coherency, the strain energy may be written per mole-O in the oxide as [12,13]

$$u = \frac{V_m}{2}\frac{Y}{1-\nu}\varepsilon(x)^2, \tag{3}$$

where V_m, Y, ν, and $\varepsilon(x)$ denote the molar volume, Young's modulus, Poisson's ratio, and strain at a position x in the reaction product ZrO_2, respectively. Obviously, $\varepsilon(x)$ will die out with distance x and hence, the strained region in the oxide in front of the interface will be spatially limited. For simplicity sake, we assume here that ∇u be constant irrespective of the oxide thickness, ξ. This implies that $\varepsilon(x)$ decays parabolically with distance x from the interface, $x = 0$.

One may assume steady-state or $\nabla J_O \approx 0$ [15], and integrate Eq. (1) to obtain

$$J_O = -\frac{\bar{L}}{\xi}\Delta\mu_O - \bar{L}\nabla u, \tag{4}$$

where $\bar{L}$ is the spatial average of L across the reaction product and $\Delta\mu_O = \mu''_O - \mu'_O$. Assuming that the interfacial reaction between gaseous oxygen and ZrO_2 is fast enough (so that the overall kinetics is governed by solid-state diffusion), one may set

$$\Delta\mu_O = \frac{1}{2}\Delta G, \tag{5}$$

where ΔG is the free energy change of the reaction

$$Zr + O_2 = ZrO_2. \tag{6}$$

Due to mass conservation, one has

$$J_O = -\frac{2}{V_m}\frac{d\xi}{dt}, \tag{7}$$

where ξ stands for the thickness of the ZrO_2 as measured from the Zr/ZrO_2 interface ($x = 0$) (see Fig. 1) and t the time duration. By associating Eqs. (4), (5) and (7), one finally obtains a kinetic equation

$$\frac{d\xi}{dt} = \frac{K_p}{\xi} - \beta \tag{8}$$

or upon integration with the initial condition, $\xi(t = 0) = 0$,

$$t = -\frac{\xi}{\beta} - \frac{K_p}{\beta^2}\ln\left(1 - \frac{\beta}{K_p}\xi\right), \tag{9}$$

where

$$K_p \equiv \frac{\bar{L}V_m}{4}(-\Delta G); \quad \beta \equiv \frac{\bar{L}V_m}{2}(-\nabla u). \tag{10}$$

One can easily show that as β approaches 0, Eq. (9) reduces to the conventional, parabolic rate law, $\xi^2 = 2K_p t$. It is emphasized that the mechanically driven diffusion is in the opposite direction to the chemically driven diffusion. This counter effect causes the overall kinetics to deviate from the conventional parabolic kinetics.

3. Experimental

Rectangular plates of Zr (99.9% purity, CEZUS, France), measuring ca. (8–12) mm × (6–16) mm × (0.8–1) mm and weighing (0.2–1) g, were employed as specimens. All the surfaces of each plate were polished with diamond pastes of grit size down to 1 μm, washed with acetone followed by distilled water, and then in an aqueous solution of $5\%HF + 45\%HNO_3$ and subsequently in distilled water again.

Oxidation experiment was carried out in a fixed atmosphere of air in a temperature range of 400–800 °C by thermogravimetry (TGA). A plate specimen was hung down from a thermobalance into a built-in (graphite) furnace whose temperature was previously set at a temperature of interest (within ±1 °C) and its mass increase was monitored in situ against time by the thermobalance with a ±1 μg resolution (Setaram TG-DTA 92-18, France).

In order to get a further insight into the defect-chemical nature of the reaction product, ZrO_2, the open-circuit potential across the reaction product was measured from a galvanic cell with the configuration

$$Pt|Zr|ZrO_2|O_2(air), Pt. \quad (I)$$

A Zr-plate was first oxidized within the pre-transition period and then a corner of the plate was abraded to expose the base metal, Zr. A Pt-wire of 0.2 mm thickness was tightly wound around the corner (where the oxide layer was scraped off) to secure an electrical contact between the Zr–metal and the Pt-wire and another wire around the opposite corner where the oxide layer remained. The corner of the plate, where the Zr/Pt contact was formed, was embedded sufficiently deep into a densely packed, fine glass powder (with the softening point of ca. 690 °C) in an alumina cup. The entire assembly was subsequently put into a furnace that had already been at 700 °C. By quickly melting the glass covering the bare metal Zr, the oxidation of Zr could be effectively suppressed to keep the Zr/Pt contact for a reasonably long period of time. The voltage between the two Pt-lead wires was measured against surrounding oxygen partial pressure at a fixed temperature of 700 °C. The oxygen partial pressure in the surrounding of the cell was monitored by a ZrO_2-based oxygen sensor.

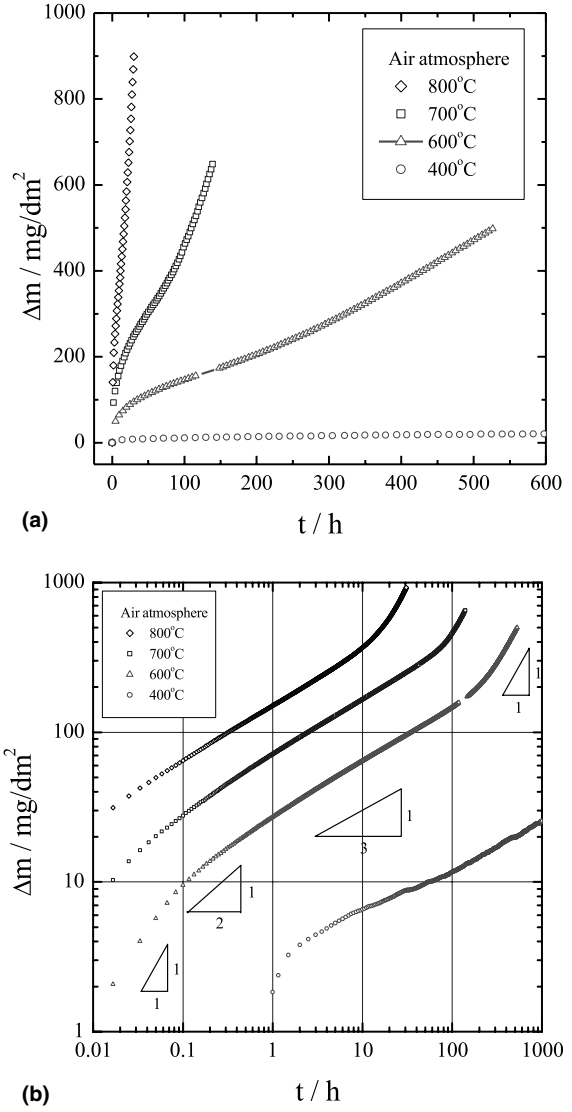

Fig. 2. Mass gain per unit area, Δm vs. exposure time, t to air at different temperatures in a linear scale (a) and in a log–log scale (b). The sequence of small triangles shows the slopes 1, 1/2, 1/3 and 1 in order.

4. Results and discussions

4.1. Oxidation kinetics

Fig. 2(a) shows the TGA results, mass gain per unit area (Δm) relative to the initial mass m_0 vs. exposure time (t) at different temperatures in the air atmosphere. The mass gain particularly at 600 °C displays all the typical features in both pre-transition and post-transition periods, which re-confirms what have been repeatedly observed [1,2]. Conventionally the oxidation kinetics has been represented as [2]

$$(\Delta m)^n = Kt, \quad (11)$$

with the reaction order, n and appropriate rate constant, K. We, thus, re-plot Fig. 2(a) in a log–log scale in Fig. 2(b). One can now better see, say, from the 600 °C isotherm that kinetics look initially linear or $n \approx 1 (t < 0.1$ h), then apparently cubic or $n \approx 3$ up to

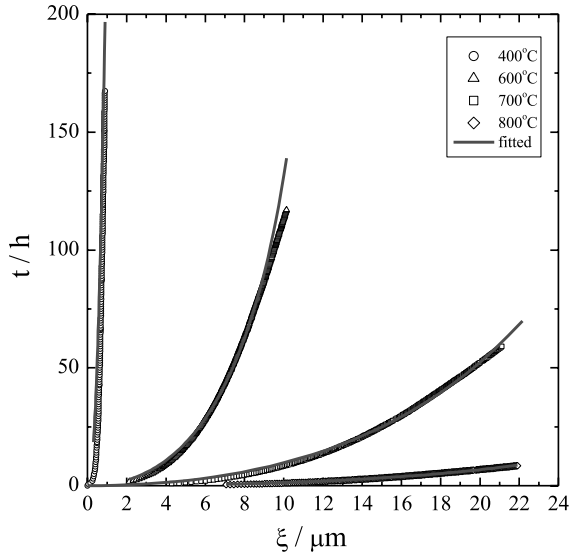

Fig. 3. ZrO_2 thickness, ξ vs. exposure time, t. The solid curves are the best fitted to Eq. (9) in the text.

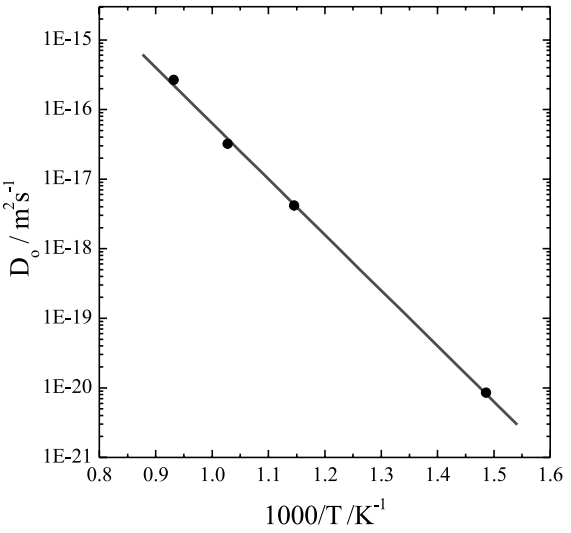

Fig. 4. Intrinsic diffusivity of oxygen, D_O vs. reciprocal temperature.

the breakaway (at $t \approx 100$ h) from which the kinetics turn linear again. It should be noted that one can argue that there is a region of parabolic kinetics before completely turning to the cubic kinetics.

The mass-gain data before the breakaway in Fig. 2(a) have now been non-linear least-squares (NLLS) fitted to Eq. (9). In this procedure, the mass gain was first transformed to the thickness of the growing oxide as $\xi = \Delta m V_m / 2M_O$, where M_O is the atomic weight of oxygen and V_m has been taken as that for t-ZrO_2 or $V_m = 2.10 \times 10^{-5}$ m^3 mol^{-1}. The fitted results are depicted by the solid curves in Fig. 3 with the fitting parameters, K_p and β as listed in Table 1. As is seen, Eq. (9) is describing the mass gain quite satisfactorily, supporting its validity or truthfulness.

4.2. Intrinsic diffusivity

The reaction free energy, ΔG for Zr-oxidation in air ($P_{o_2} = 0.21$ atm) is known [14] as listed in the fourth row of Table 1 at each temperature of examination. One can thus derive from Eq. (2) with $C_O \approx 2/V_m$ and Eq. (10) the average intrinsic diffusion coefficient of component oxygen, $\bar{D}_O$. The results are listed in the fifth row of Table 1 and plotted against reciprocal temperature in Fig. 4. The average intrinsic diffusivity of component oxygen may best be represented as

$$\bar{D}_O/\mathrm{m}^2\ \mathrm{s}^{-1} = (6.3^{+4.7}_{-2.7}) \times 10^{-9} \exp\left(-\frac{1.59 \pm 0.04\ \mathrm{eV}}{kT}\right) \quad (12)$$

with a linear correlation coefficient $r = -0.9993$ between $\ln D_O$ and $1/T$ for the four data entries.

As already expected from the dark color of the oxide scale, the open-circuit potential of Cell (I) indicates that the oxide is indeed a mixed ionic electronic conductor. As is seen in Fig. 5, the open-circuit potential across the oxide is 1.28 V when $P_{o_2} = 1$ atm. (When the surrounding P_{o_2} was changed to an N_2/O_2 mixture gas and left alone to see the time-dependence of EMF, the EMF started in a while to fluctuate more or less in a regular interval. After some intervals, EMF vanished. It was due

Table 1
Analysis results of Zr-oxidation kinetics on the basis of Eq. (9) in the text

T/K	673	873	973	1073
K_p (m^2 h^{-1})	$(2.6693 \pm 0.0009) \times 10^{-15}$	$(9.47 \pm 0.04) \times 10^{-13}$	$(6.40 \pm 0.03) \times 10^{-12}$	$(4.722 \pm 0.019) \times 10^{-11}$
β (m h^{-1})	$(1.078 \pm 0.007) \times 10^{-9}$	$(7.51 \pm 0.07) \times 10^{-8}$	$(1.80 \pm 0.02) \times 10^{-7}$	$(1.247 \pm 0.013) \times 10^{-6}$
$\lvert\Delta G\rvert$ (J)	9.60×10^5	9.20×10^5	9.00×10^5	8.81×10^5
$\bar{D}_O$ (m^2 s^{-1})	8.56×10^{-21}	4.15×10^{-18}	3.20×10^{-17}	2.66×10^{-16}
$\nabla\varepsilon$ (J m^{-1} mol^{-1})	2.00×10^{11}	3.65×10^{10}	1.27×10^{10}	1.16×10^{10}
ξ_c (m)	–	1.31×10^{-5}	2.32×10^{-5}	2.73×10^{-5}
$u(0)$ (J mol-O^{-1})	–	4.78×10^5	2.94×10^5	3.17×10^5

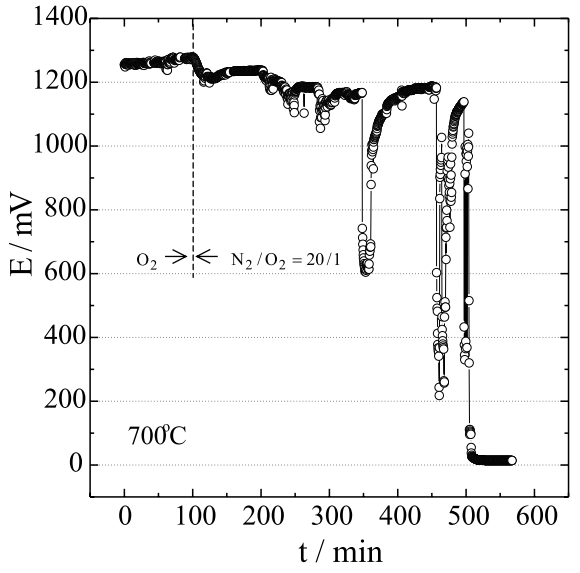

Fig. 5. The open-circuit potential E of Cell (I) vs. time in different oxygen partial pressures.

to the failure of the cell, that is, the loss of Zr/Pt contact due to the re-oxidation of the Zr metal in contact with the Pt-lead wire. As a consequence, the EMF could not be measured in the air atmosphere. This electrochemical study will make the subject of a forthcoming publication.) The open-circuit potential, E, of Cell (I) is given as [15]

$$E = \frac{1}{4F}\int_{\mu'_{O_2}}^{\mu''_{O_2}} t_{ion}\mathrm{d}\mu_{O_2}, \tag{13}$$

where F is the Faraday constant and t_{ion} the ionic transference number. Introducing an average ionic transference number, $\bar{t}_{ion}$, of the reaction product or over the oxygen potential interval, one may rewrite Eq. (13) as

$$E = \frac{\bar{t}_{ion}}{4F}(\mu''_{O_2} - \mu'_{O_2}) = \frac{\bar{t}_{ion}}{4F}(-\Delta G). \tag{14}$$

In the present measurement, the oxygen partial pressure in the surrounding is $P_{o_2} = 1$ atm and hence, $\mu''_{O_2} = \mu^0_{O_2}$, the standard chemical potential of gas oxygen. It therefore follows that $\Delta G = \Delta G^0$, the standard reaction free energy. At 700 °C, $\Delta G^0 = -9.15 \times 10^5$ J/mol-O_2 [14]. If the zirconia in present concern were an exclusively ionic conductor or $t_{ion} \approx 1$, one would have an open-circuit potential of $E_N = 2.37$ V, but the experimental value is only 1.28 V. Thus, the mean ionic transference number across the reaction product is expected from Eq. (14) to be

$$\bar{t}_{ion} = \frac{E}{E_N} \approx 0.54. \tag{15}$$

Taking into account that the reaction-free energy in air atmosphere ($P_{o_2} = 0.21$ atm) is very close to the standard reaction-free energy (see Table 1), the open-circuit potential even at $P''_{o_2} = 0.21$ atm should be close to 1.28 V and hence, the mean ionic transference number should also be close to 0.5. This confirms that the reaction product ZrO_2 is a mixed ionic electronic conductor.

The oxidation, therefore, proceeds via a coupled diffusion of the charged components, oxide anions (O^{2-}) and electrons (e^-), and hence, the intrinsic diffusion coefficient in Eq. (2) may be a Planck-type combination of the average partial conductivities of the two charged components, $\bar{\sigma}_{O^{2-}}$ and $\bar{\sigma}_{e^-}$, respectively, or [16]

$$\bar{D}_O = \frac{V_m RT}{8F^2}\frac{\bar{\sigma}_{O^{2-}}\bar{\sigma}_{e^-}}{\bar{\sigma}_{O^{2-}} + \bar{\sigma}_{e^-}}. \tag{16}$$

Nonetheless, it cannot be said at this point whether these partial conductivities are due to bulk or grain boundaries. Obviously more work is required to elucidate this issue.

4.3. Protective-layer thickness

We have a priori conjectured that the oxide is subjected to a constant, compressive (in-plane) stress gradient. In order for a compressive stress to keep t-ZrO_2 stable below the normal transition temperature to m-ZrO_2 (1205 °C), the compressive strain-energy gain with the former over the latter should be no smaller than the volume-free energy difference between t-ZrO_2 and m-ZrO_2 at temperatures of interest or

$$u(\text{m-}ZrO_2) - u(\text{t-}ZrO_2) \geqslant \mu(\text{t-}ZrO_2) - \mu(\text{m-}ZrO_2). \tag{17}$$

Assuming the heat capacities of the two polymorphs are independent of temperature, one can estimate from the enthalpy of transformation of ZrO_2, $\Delta H_{tr} = 5.9 \times 10^3$ J mol^{-1} [17] the lower bound of the strain energy difference as 2.4×10^3 J mol^{-1} at e.g., 600 °C. It can, thus, be easily recognized that the stability condition, Eq. (17) is satisfied up to a certain, critical thickness, ξ_C of the reaction product. If this compressive strain is attributed to the interfacial coherency at the Zr/ZrO_2 interface, the critical thickness is expected to remain more or less constant under the given interfacial condition at a fixed temperature. The thickness of the protective layer has actually been reported to be approximately constant on the order of 2–3 μm [2,3] at temperatures where Zircaloy is normally used. It is, however, expected that as the free energy difference (the right-hand side of Eq. (17)) gets smaller with increasing temperature, the critical thickness increases with temperature as the mechanical property of solid is rather insensitive to temperature. This prediction seems to be

supported by Fig. 2(b) where the weight gain or thickness to the transition point increases with temperature.

Once the reaction product surpasses the critical thickness ξ_C, the thermodynamically stable m-ZrO_2 tends to form upon the surface of t-ZrO_2. Due to the larger volume of m-ZrO_2, the underlying t-ZrO_2 is subjected to an incipient tensile stress and this tensile stress may trigger cracks to be initiated. As the oxidation proceeds, the crack tips move along with the moving ZrO_2/Zr interface because of continual transformation to m-ZrO_2 at the crack tips. The transformation is expected to occur everywhere upon the exposed surface of cracks. One may, thus, expect a fractal-like growth of cracks, eventually leading to a network of fissures in otherwise the tetragonal region of $x \geqslant \xi_C$. This seems to be in agreement with the experimental observation of the microstructure [3]. It is thus speculated that the breakaway may be attributed to the phase transition accompanied by crack formation.

4.4. Strain energy

We will next evaluate the strain-energy gradient, ∇u, that was assumed to be constant, from the ratio of β to K_p in accord with Eq. (10). The results are given in the sixth row of Table 1. As a first-order approximation, let us assume that the strain energy vanishes at $x = \xi_C$ instead of a finite value such as in Eq. (17). The critical thickness corresponding to the transition point, ξ_C can now be estimated from Fig. 2(b) as 13, 23 and 27 μm at 600, 700, and 800 °C, respectively (the seventh row in Table 1). (It cannot be evaluated at 500 °C, see the figure.) Now that we know the strain-energy gradient and the critical thickness corresponding to $u = 0$, we can estimate the strain energy/mol-O right at the metal/oxide interface ($x = 0$) as $u(0) = \nabla u \times \xi_C$. The results are shown in the eighth row of Table 1. They are on the order of 10^5 J mol-O^{-1} or 10^{10} J m^{-3}, insensitive to temperature, which is quite reasonable [8].

One may estimate from $u(0)$ the magnitude of the compressive strain there, $\varepsilon(0)$. Young's modulus of ZrO_2 at the temperatures of interest is not immediately available. Thus assuming that it is not much different from that of stabilized zirconia, we take the value for sintered, stabilized zirconia [18], $Y = 2 \times 10^{11}$ Pa and $\nu = 0.3$. Eq. (3) then yields a strain value, $\varepsilon(0) \approx -0.3$ irrespective of temperature.

ZrO_2 has a Pilling–Bedworth-ratio of 1.48 (t-ZrO_2) or 1.51 (m-ZrO_2). The interfacial coherency, be the Zr/ZrO_2 interface coherent or semi-coherent, may thus be a cause of compressive stress. Assuming the interface being coherent, the coherency strain is calculated as $\varepsilon(0) \approx 0.4$ simply by using the values for the lattice parameters of hexagonal Zr (a-axis, 0.5039 nm) and t-ZrO_2 (a-axis, 0.364 nm) [19]. Tantalizingly, the latter is so close to the value evaluated in the present work, $\varepsilon(0) = -0.3$, even though the value is obviously too large for a coherency strain.

The compressive stress may also be attributed to the increased non-stoichiometry (δ) at the $Zr/ZrO_{2-\delta}$ interface. It is known [20,21] that the lattice of an oxide, e.g., $CeO_{2-\delta}$ and $La_{0.7}Ca_{0.3}CrO_{3-\delta}$, expands with increasing oxygen-vacancy concentration or non-stoichiometry (δ). A compressive stress should thus develop at the reduced side of an oxide due to the lattice coherency (often called chemically-induced stress [20]). For the case of $CeO_{2-\delta}$ [20], the compressive strain per non-stoichiometry amounts to $\eta(\equiv \varepsilon/\delta) = 0.11$ to 0.23 at 1000 °C. At the very $Zr/ZrO_{2-\delta}$ interface, the oxide is the most reduced or δ takes the maximum possible value at the given temperature. The oxygen non-stoichiometry of t-$ZrO_{2-\delta}$ and m-$ZrO_{2-\delta}$ has recently been reported [22] against oxygen partial pressure only in a limited range of $10^{-11} < P_{O_2}/\text{atm} < 1$ at elevated temperatures (900–1400 °C). It is hardly justified to extrapolate the reported data far outside the range of observation to estimate the non-stoichiometry of $ZrO_{2-\delta}$ in equilibrium with Zr (where the equilibrium oxygen partial pressure is $10^{-56}, 10^{-49}$, and 10^{-44} at 600, 700 and 800 °C, respectively). Nevertheless, we attempted for m-$ZrO_{2-\delta}$ to obtain the values $\delta \approx 1.8$, 1.4, 1.1 at 600, 700 and 800 °C, respectively. Taking, on the basis of structural similarity, the value of $\eta(\equiv \varepsilon/\delta)$ for $ZrO_{2-\delta}$ as that of $CeO_{2-\delta}$ or $\eta = 0.11$ to 0.23, one can get the lattice coherency strain as $\varepsilon(0) = 0.12$ to 0.41. It is again surprising that this value is similar to the value $\varepsilon(0) = -0.3$ that has been evaluated in the present analysis, hinting the origin of the compressive stress.

The estimated value $\varepsilon(0) \approx -0.3$ corresponds to a compressive stress of about 60 GPa. It is roughly two orders of magnitude higher than both the measured value [3] and the load carrying capability of Zr–metal substrate. This discrepancy may be attributed to the surface tension of t-ZrO_2. It has been shown that t-ZrO_2 can exist indefinitely at room temperature when the crystallite size is smaller than the critical value of about 30 nm [7]. A high resolution TEM study [23] indeed shows the presence of t-ZrO2 at such a small size in the close vicinity of the Zr/ZrO_2 interface. Clearly more work is required to elucidate this issue.

5. Concluding remarks

We now conclude that the oxidation kinetics of Zircaloy can be satisfactorily described by introducing a constant (compressive) strain-energy gradient as a diffusional driving force in addition to the chemical potential gradient of component oxygen as

$$\frac{d\xi}{dt} = \frac{K_p}{\xi} - \beta \text{ or } t = -\frac{\xi}{\beta} - \frac{K_p}{\beta^2} \ln\left(1 - \frac{\beta}{K_p}\xi\right). \tag{18}$$

This kinetic equation yields an intrinsic diffusion coefficient of component oxygen and compressive strain energy of reasonable magnitudes. The reaction product, ZrO_2 is a mixed ionic electronic conductor with the ionic transference number of ca. 0.5 and, hence, the oxygen diffusion coefficient is of the Planck-type. The hypothesis enables one to predict the thickness of the reaction product till the breakaway and the microstructure evolution of the oxide therefrom. It is suggested that the compressive stress is due to the interfacial and/or lattice coherency. Once the strain-energy distribution is elaborated, the theory may be improved further.

Acknowledgements

The first author is very much indebted to Professor J. Mizusaki at Tohoku University, Japan, Professors B.J. Wuensch, H.L. Tuller, and L. Hobbs all at Massachusetts Institute of Technology, USA for enlightening discussions.

References

[1] T. Ahmed, L.H. Keys, J. Less-Common Met. 39 (1975) 99.
[2] E. Hillner, in: Zirconium in the Nuclear Industry: Third International Symposium, ASTM STP, vol. 633, 1977, p. 211.
[3] H.-J. Beie, A. Mitwalsky, F. Garzarolli, H. Ruhmann, H.-J. Sell, in: Zirconium in the Nuclear Industry: Tenth International Symposium, ASTM STP, vol. 1245, 1994, p. 615.
[4] F. Garzarolli, H. Seidel, R. Tricot, J.P. Gros, in: Zirconium in the Nuclear Industry: Ninth International Symposium, ASTM STP, vol. 1132, 1991, p. 395.
[5] J. Godlewski, in: Zirconium in the Nuclear Industry: Tenth International Symposium, ASTM STP, vol. 1245, 1994, p. 663.
[6] J. Godlewsky, J.P. Gros, M. Lambertin, J.F. Wadier, H. Weidinger, in: Zirconium in the Nuclear Industry: Ninth International Symposium, ASTM STP, vol. 1132, 1991, p. 416.
[7] R.C. Garvie, J. Phys. Chem. 82 (1978) 218.
[8] L. Hobbs, private communication.
[9] H.E. Evans, D.J. Norfolk, T. Swan, J. Electrochem. Soc. 125 (1978) 1180.
[10] A.P. Zhilyaev, J.A. Szpunar, J. Nucl. Mater. 264 (1999) 327.
[11] D.L. Douglass, C. Wagner, J. Electrochem. Soc. 113 (1966) 671.
[12] H. Schmalzried, Chemical Kinetics of Solids, VCH, Weinheim, 1995 (Chapter 14).
[13] S.P. Timoshenko, J.N. Goodier, in: Theory of Elasticity, 3rd Ed., McGraw-Hill, New York, 1970, p. 247.
[14] L.B.Pankratz, Thermodynamic Properties of Elements and Oxides, PB83-174052, US Bureau of Mines, Albany, OR, 1983.
[15] C. Wagner, Z. Phys. Chem. B 21 (1933) 25.
[16] H. Schmalzried, Solid State Reactions, Verlag Chemie, Weinheim, 1981 (Chapter 6).
[17] E.D. Whitney, J. Am. Ceram. Soc. 45 (1962) 612.
[18] M. Barsoum, in: Fundamentals of Ceramics, McGraw-Hill, New York, 1997, p. 401.
[19] JCPDS, 26-1399 and 42-1164, International Center for Diffraction Data.
[20] A. Atkinson, T.M.G.M. Ramos, Solid State Ionics 129 (2000) 259.
[21] I. Yasuda, M. Hishinuma, in: M. Dokiya, O. Yamamoto, H. Tagawa, S.C. Singhal (Eds.), Proceedings of 4th International Symposium on Solid Oxide Fuel Cells (SOFC-IV), The Electrochemical Society, 1995, p. 924.
[22] J. Xue, J. Electrochem. Soc. 138 (1991) 36C.
[23] H. Anada, K. Takeda, in: Zirconium in the Nuclear Industry: Eleventh International Symposium, ASTM STP, vol. 1295, 1996, p. 35.